Synthesis, structure and noncovalent interactions of mesityl(phenyl)phosphine oxide glycolate based hydrogen-bonded nanosized organic framework

Alexey A. Kagilev[1,a], Ilyas F. Sakhapov[1,b], Zufar N. Gafurov[1,c], Artyom O. Kantyukov[1,2,d],
Ilya K. Mikhailov[1,e], Daut R. Islamov[3,f], Alexander V. Gerasimov[2,g], Oleg A. Filippov[4,h],
Aidar T. Gubaidullin[1,j], Olga S. Soficheva[1,k], Oleg G. Sinyashin[1,l], Dmitry G. Yakhvarov[1,2,m]

[1]Arbuzov Institute of Organic and Physical Chemistry, FRC Kazan Scientific Center, Russian Academy of Sciences, 420088, Kazan, Russian Federation

[2]A.M. Butlerov Institute of Chemistry, Kazan Federal University, 420008, Kazan, Russian Federation

[3]Laboratory for Structural Studies of Biomacromolecules, FRC Kazan Scientific Center, Russian Academy of Sciences, 420111, Kazan, Russian Federation

[4]A.N. Nesmeyanov Institute of Organoelement Compounds, Russian Academy of Sciences, 119991, Moscow, Russian Federation

[a]al-kagilev@mail.ru, [b]ilyas.sakhapov@iopc.ru, [c]gafurov.zufar@iopc.ru, [d]kant.art@mail.ru, [e]tiimhailovilya@gmail.com, [f]daut1989@mail.ru, [g]Alexander.Gerasimov@kpfu.ru, [h]h-bond@ineos.ac.ru, [j]aidar@iopc.ru, [k]myaolechka@yandex.ru, [l]oleg@iopc.ru, [m]yakhvar@iopc.ru

Corresponding author: D. G. Yakhvarov, yakhvar@iopc.ru

ABSTRACT The reaction of glyoxylic acid monohydrate with mesityl(phenyl)phosphine in air led to the formation of mesityl(phenyl)phosphine oxide glycolate. The synthesized mesityl(phenyl)phosphine oxide glycolate has been characterized by various analytical methods including X-ray crystal structure analysis. The analysis of intermolecular interactions in the crystal revealed interesting modes of the noncovalent bonding between pairs of molecules. These intermolecular interactions cause the formation of one-dimensional cylindrical channels with diameter of 1 nm (10 Å) and provide the crystal with the properties of precise nano-sized crystalline porous material which can be served as the component for precise nanofiltration membranes improving the properties of amorphous polymers which suffer from disordered pore structures and reduced selectivity towards separating molecules.

KEYWORDS phosphine, phosphine oxide, glycolate, X-ray diffraction, noncovalent bonding

1. Introduction

Covalent and noncovalent interactions, including hydrogen bonds, are objects of extensive study in the global scientific literature [1–7]. The significant interest in utilizing hydrogen bonding to construct ordered crystalline networks has prompted extensive research into hydrogen-bonded organic frameworks (HOFs). These frameworks rely on the assembly of organic building blocks through hydrogen-bonding interactions, enabling the formation of two-dimensional (2D) and three-dimensional (3D) crystalline nanosized networks [8]. Such a hydrogen-bonded nanocrystalline structures has gained a great attention during the past decade mostly due to their applications in the fields of catalysis, energy, biochemistry as well as the storage and separation of fine chemicals [4, 9–14]. Due to the weakness of single hydrogen bond, the stability of HOF can be significantly improved by creating multiple intermolecular forces including $\pi\cdots\pi$ and $CH\cdots\pi$ interactions. Whereas, examples of $C–H\cdots C$ contacts are rather unusual and are rarely invoked in the description of nanomolecular aspects of crystal structures [15–19]. At the same time, these types of weak hydrogen bonds play an important role in the formation of some intricate 3D supramolecular networks [20]. Nevertheless, one of the basic

hydrogen bonding synthesizer motifs used to design HOFs is O–H···O interaction involving carboxylic acid group (–COOH), which presence, however, often causes polymorphism due to the flexibility of hydrogen bonds [13]. It should be also noted, that examples of phosphorus-based HOFs are rather uncommon in published literature, although P = O groups of phosphine oxides are also known to form stable hydrogen bonds with diverse substance classes [21–24]. The interest of our research group is focused on the synthesis of organophosphorus compounds, including unsymmetrically substituted phosphines and phosphine oxides [25], which are commonly applied in asymmetric synthesis, both as chiral ligands [26–28] and as organocatalysts [29–33].

2. Experimental

2.1. Materials and measurements

Diethyl ether was dried by standard method and freshly distilled before use. Glyoxylic acid monohydrate was purchased from Sigma-Aldrich and used as received without further purification. Mesityl(phenyl)phosphine was prepared according to the published procedure [34]. NMR spectra were recorded using a Bruker MSL-400 spectrometer. ^{1}H and ^{13}C$\{^1$H$\}$ chemical shifts are reported in parts per million (ppm) downfield of tetramethylsilane and were calibrated against the residual resonance of the deuterated solvent, whereas ^{31}P and ^{31}P$\{^1$H$\}$ NMR spectra are referenced to an external 85 % H_3PO_4 sample (0 ppm). Elemental analysis was performed on a EuroVector CHNS-O Elemental Analyser EA3000.

Data set for single crystal of mesityl(phenyl)phosphine oxide glycolate was collected on a Rigaku XtaLab Synergy S instrument with a HyPix detector and a PhotonJet microfocus X-ray tube using Cu Kα (1.54184 Å) radiation at low temperature (100.0(2) K). Images were indexed and integrated using the CrysAlisPro data reduction package. Data were corrected for systematic errors and absorption using the ABSPACK module: numerical absorption correction based on Gaussian integration over a multifaceted crystal model and empirical absorption correction based on spherical harmonics according to the point group symmetry using equivalent reflections. The GRAL module was used for analysis of systematic absences and space group determination. The structure was solved by direct methods using SHELXT [35] and refined by the full-matrix least-squares on F^2 using SHELXL [36]. Non-hydrogen atoms were refined anisotropically. The hydrogen atoms were inserted at the calculated positions and refined as riding atoms. A solvent mask was calculated and 156 electrons were found in a volume of 756Å^3 in one void per unit cell. This is consistent with the presence of 0.5 [CH_3OH] per asymmetric unit which account for 162 electrons per unit cell. The figures were generated using Mercury 4.1 program [37]. CCDC 2093649 contains the supplementary crystallographic data for this paper. These data can be obtained free of charge via [38].

The powder diffractograms were obtained on a Bruker D8 Advance automatic X-ray diffractometer equipped with a Vario attachment and a Vantec linear coordinate detector. Cu Kα1 radiation (λ 1.54063 Å), monochromatized with a bent Johansson monochromator, 40 kV, 40 mA X-ray tube mode was used. The experiments were performed at room temperature in Bragg-Brentano geometry with a flat sample. The sample was applied to the surface of a standard silicon plate reducing background scattering. The diffractograms were recorded in the range of scattering angles 2–80°, step 0.008°, time of the spectrum acquisition at the point 0.1–0.5 sec. The results of 8 scans were summed up, so that the total set time was equal to 1.2 sec per step. The data have been processed using the EVA software package [39].

Simultaneous thermal analysis was carried out using Simultaneous Thermal Analyzer – STA 449 F1 Jupiter® (Netzsch). All studies were carried out in an argon atmosphere with a flow rate of 75 ml/min and a heating rate of 10 °C/min. The measurements were taken in the temperature range from 40 to 350 °C. For experiments, 5.6 mg sample was placed in aluminium crucibles (40 μL) with lids having 3 holes, each of 0.5 mm in diameter.

The interactions in the crystal were analyzed with the CrystalExplorer program [40]. There are 15 neighbors for single molecule of **1**. Due to the symmetry of the crystal, there are only nine unique modes of the interaction between pairs of molecules. The energies of the pairwise interaction were computed under the approach parametrized in the CrystalExplorer [41] on the B3LYP/6-31G(d,p) level and provided in Table 1.

2.2. Preparation of mesityl(phenyl)phosphine oxide glycolate (1)

A solution of glyoxylic acid monohydrate (100 mg, 1.0 mmol) in 10 mL of diethyl ether was added to a solution containing mesityl(phenyl)phosphine (0.2 mL, 1.0 mmol) in 10 mL of diethyl ether. After the addition of glyoxylic acid monohydrate, the flask was opened to air and stirred for 24 hours at room temperature, after which the formation of a white precipitate was observed. The resulting precipitate was filtered, washed with diethyl ether and dried under vacuum. The yield was 223 mg (70 %).

^{1}H NMR (400.17 MHz, DMSO-D$_6$, 300 K):δ (ppm) = 2.28 (s, 3H, *p*-CH$_3$ of Mes), 2.47 (s, 6H, *o*-CH$_3$ of Mes), 3.62 (s, 1H, PCOH), 5.27 (d, ^{2}J$_{PH}$ = 6.1 Hz, 1H, PCH), 6.91 (s, 2H, *m*-H of Mes), 7.40–7.51 (m, 2H, *o*-H of Ph), 7.80–7.83 (m, 3H, *m*-. *p*-H of Ph). ^{13}C$\{^1$H$\}$ NMR (100.62 MHz, DMSO-D$_6$, 300 K): δ = 20.05 (s, *p*-CH$_3$ of Mes), 22.68 (s, *o*-CH$_3$ of Mes), 72.89(s, PCH), 127.99 (d, ^{3}J$_{PC}$ = 11.8 Hz, *m*-CH of Mes), 130.53 (d, ^{3}J$_{PC}$ = 11.6 Hz, *m*-CH of Ph), 131.02 (d, ^{1}J$_{PC}$ = 12.5 Hz, *i*-C of Ph), 135.69 (s, *o*-CH of Ph), 141.35 (s, *p*-CH of Ph), 143.93 (d, ^{1}J$_{PC}$ = 10.2 Hz, *i*-C of Mes), 170.36 (d, ^{2}J$_{PC}$ = 10.6 Hz, COOH). ^{31}P$\{^1$H$\}$ NMR (161.70 MHz, DMSO-D$_6$, 300 K):δ (ppm) = 39.27 (s).

Anal. (%) calcd. for $C_{17}H_{19}O_4P$ (318.29): C, 64.15; H, 6.02. Found: C, 64.10; H, 6.01.

3.   Results and discussion

In this article, we report on the synthesis, crystal structure analysis and hydrogen bonding motifs of a mesityl(phenyl)phosphine oxide glycolate **1** which forms hydrogen-bonded nanosized organic framework (Fig. 1).
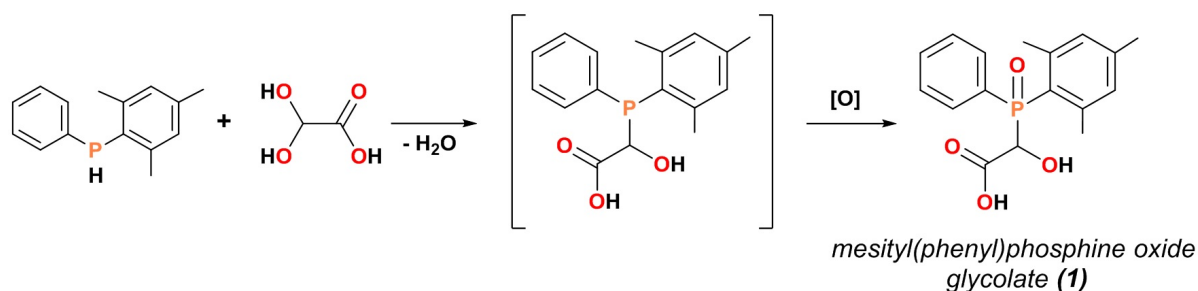

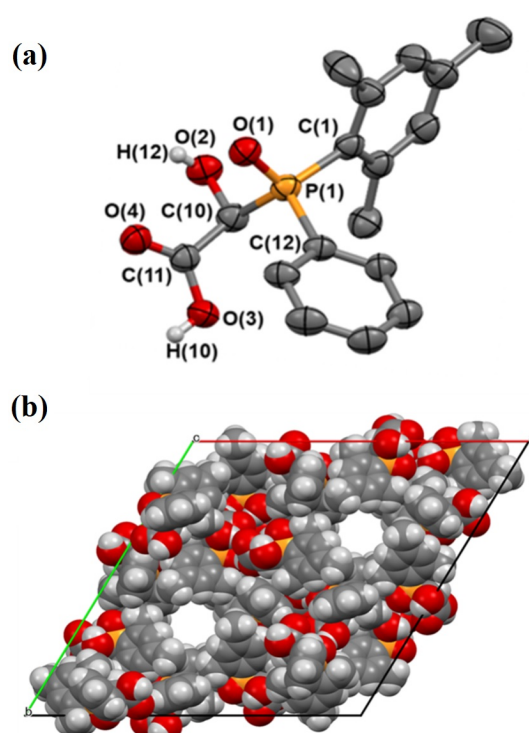FIG. 1.   Scheme 1. Synthesis of mesityl(phenyl)phosphine oxide glycolate **1**

FIG. 2.   The solid-state molecular structure of mesityl(phenyl)phosphine oxide glycolate (thermal ellipsoids at the 50 % probability level, hydrogen atoms except those of the -OH groups are omitted for clarity) (a); its crystal packing featuring one-dimensional channels along the c axis (b)

The ^{31}P NMR spectrum recorded after stirring the reaction mixture containing mesityl(phenyl)phosphine and glyoxylic acid monohydrate in 1:1 ratio in diethyl ether as a solvent for 24 h showed a signal at $\delta_P = -8.70$ ppm attributed to mesityl(phenyl)phosphine glycolate. However, the generated species rapidly oxidizes in air with formation of a new signal at $\delta_P = 39.27$ ppm, which was ascribed to mesityl(phenyl)phosphine oxide glycolate (Scheme 1). After 6 days, the formed precipitate was redissolved in DMSO-D_6 and was analysed by ^1H, $^{31}P\{^1H\}$, ^{13}C NMR spectroscopy, which revealed the formation of **1** as analytically pure product. The thermophysical properties of **1** were investigated using synchronous thermal analysis. The results are shown in Fig. S1. The mass loss of the sample in the temperature range 40–164 °C does not exceed 3.3 % and is related to solvent removal. Subsequent steps of the mass loss are related to the thermal decomposition of the sample and are accompanied by exo-effects. In addition to the exo-effects of decomposition, the DSC curve clearly captures the endo-effect of melting with an onset temperature of 164 °C and a peak temperature of 172 °C.

The molecular structure of **1** was studied by X-ray diffraction analysis (Fig. 2a). According to powder X-ray diffraction data, the obtained mesityl(phenyl)phosphine oxide glycolate is a crystalline solid substance with well-formed crystallites and almost no amorphous component (see Fig. S2). Thus, mesityl(phenyl)phosphine oxide glycolate crystallizes
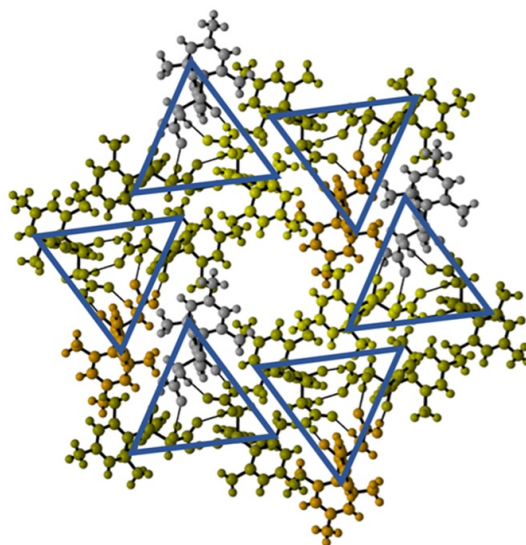
FIG. 3. Schematic representation of molecular model of a fragment of mesityl(phenyl)phosphine oxide glycolate crystal packing showing its honeycomb network
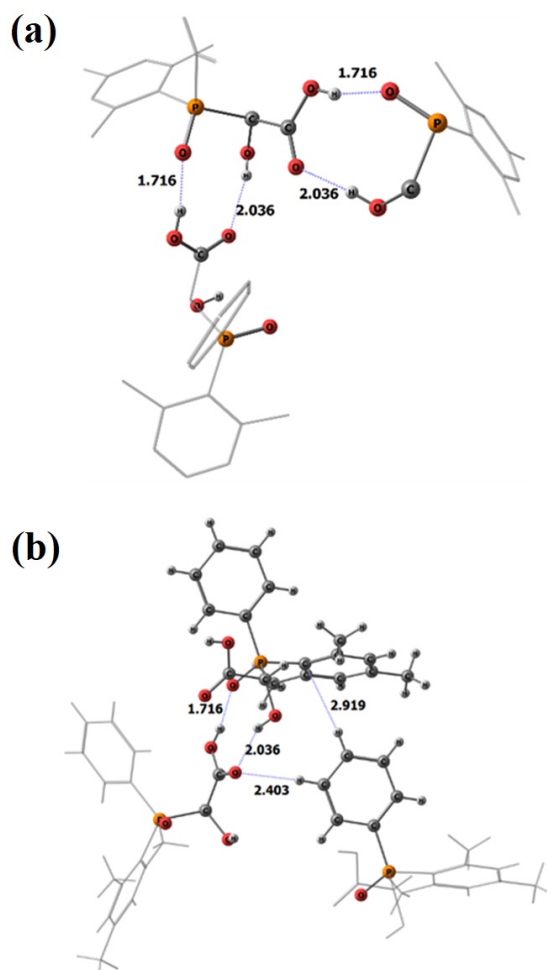

FIG. 4. Fragments of crystal packing showing two equivalent cyclic hydrogen bonds formed by each molecule of **1**, hydrogen atoms, except participated in the target hydrogen bonds are removed, carbon skeleton shown as a wireframe

TABLE 1. The results of the interaction energy analysis. Distances between centres of the interacting molecules are in Å, energies are in kJ/mol

#	distance	E_{ele}	E_{pol}	E_{disp}	E_{rep}	E_{tot}	Main interaction	type
1	8.02	−112.1	−27.6	−23.3	135.7	−75.4	OH$\cdots$O	Intra-rod
2	7.00	−11.1	−3.7	−42.2	26.3	−35.0	CH$_3\cdots\pi^{Mes}$	Inter-rod
3	6.33	−7.6	−1.6	−54.5	36.3	−34.3	CH$_3\cdots\pi^{Ph}$	Inter-rod
4	9.09	−5.4	−1.7	−26.1	16.2	−19.6	CH$^{Ph}\cdots\pi^{Mes}$	Intra-rod
5	7.84	−5.5	−1.8	−14.6	2.5	−18.3	CH$_3\cdots\pi^{Ph}$	Inter-rod
6	9.58	−6.3	−1.7	−9.0	13.7	−7.3	CH$^{Ph}\cdots$O^{carboxylic}	Intra-rod
7	11.20	−0.4	−0.3	−8.8	2.7	−6.7	vdW	Inter-rod
8	11.64	−2.3	−0.3	−1.1	0.0	−3.6	vdW	Inter-rod
9	12.11	−0.5	−0.1	−2.1	0.0	−2.5	vdW	Inter-rod

in a trigonal crystal system (space group R-3 (no. 148)) with one molecule in the asymmetric part of unit cell. The phosphorus atom displays the typical for phosphine oxides tetrahedral configuration, the Newman projection along the C(10)–P(1) bond shows that mesityl group locates in *trans*-position to the C(10)–C(11) bond, while phenyl group in *gauche*-position [torsion angles C(1)P(1)C(10)C(11) 173.26°, C(12)P(1)C(10)C(11) −54.44°]. Tetrahedral phosphorus atom of phosphine oxide with three different substituents (phenyl, mesityl and glycolate) is chiral, and actual crystal structure is a racemic. Expectedly, the P(1)–C(1) bond distance (1.826 Å), is longer than that of the P(1)–C(12) bond (1.799 Å), while the P(1)–C(10) distance is 1.863 Å. The H(10) and H(12) atoms engage into O–H$\cdots$O hydrogen bonds with O(1') and O(4') atoms on adjacent molecules in the lattice respectively [d(O(3)$\cdots$O(1')) = 2.521 Å, d(O(2)$\cdots$O(4')) = 2.791 Å]. The O$\cdots$H$\cdots$O angles are in the range of 152.6°–166.5°. Interestingly, these intermolecular interactions together with C–H$\cdots$C contacts (*vide infra*) causes the formation of one-dimensional cylindrical channels with diameter of ∼10 Å (cylindrical approximation) in the crystal, these channels are directed along the *c* crystallographic axis (Fig. 2b, 8.5 % of unit cell volume, see Fig. S3 for details).

The analysis of the interaction energies in the framework of CrystalExplorer package helps us to understand the peculiarities of the formed structure. Obviously, the strongest interaction in the crystal is a cyclic hydrogen bonds of HOC–P=O group with carboxylate fragment. Each molecule of **1** bind two neighbours via this motif. Energy of each cyclic hydrogen bonding interaction is 75.4 kJ/mol, and it is also electrostatic (Table 1), verifying the nature of this interaction [20, 42]. Actually, this type of interaction is responsible for the formation of helical chains (rods) of H-bonded molecules along the c axis. The formed rods are additionally stabilized by CH$^{Ph}\cdots$O=C and CH$^{Ph}\cdots$CC^{Mes} hydrogen bonds with 7.3 and 19.6 kJ/mol energies. Notable that there are two types of rods each formed exclusively by single enantiomer. In the packing these enantiomerically pure rods are alternating, finally forming a honeycomb-like structure of racemate (Fig. 3).

After the rods formation there are no available OH groups to form an interrod connection, so the rods packing driven by weaker interactions. Nevertheless, their energetic impact is still high, being 35 kJ/mol. The one of o-CH$_3^{Mes}$ form dimer with another molecule of 1, additionally stabilized by the same Me group protons interaction with the carboxylic OH oxygen atom, and the second o-CH$_3^{Mes}$ interacts with the o-CH^{Ph}, m-C^{Mes}, with some additional stabilization due to CH$^{Mes}\cdots$Ph hydrogen bond (Fig. 4b). Notably the shortest intermolecular distance from p-CH$_3^{Mes}$ to any carbon atom is 3.1 Å, making the CH$_3$ group in the p-position of mesityl substituent almost non-interacting and turned inside the channel. It is worth noting that the interaction of the two adjacent mesityl(phenyl)phosphine oxide glycolates responsible for the interrod interaction in the crystal (see Fig. S4a). Also, the interaction energy between the two mesityl(phenyl)phosphine oxide glycolates is due to a Van der Waals dimer (E_{int} = −18.3 kJ/mol, of which only −5.5 kJ/mol is electrostatic) where CH$_3^{Mes}\cdots$Ph interaction (2.86 Å) could be revealed (see Fig. S4b, S5 and Table 1 for details).

4. Conclusion

In summary, the unsymmetrically substituted organophosphorus compound mesityl(phenyl)phosphine oxide glyco-late (**1**) has been synthesised from glyoxylic acid monohydrate and mesityl(phenyl)phosphine using *one pot* condensation approach with good yield of 70 %. The structure characterization of **1** by means of single crystal X-ray analysis revealed the one-dimensional cylindrical channels with diameter of *ca.* ∼1 nm (10 Å) in the crystal. Channels are formed by honeycomb like aggregation of six three-pointed star shaped spiral rods. Each rod formed by single enantiomer via strong cyclic hydrogen bonds, whereas CH$_3$ groups of mesityl fragment are responsible for the joining of the alternating

enantiomerically pure rods into a racemic pack providing precise nano-sized channels. Such crystalline porous materials with precise nano-sized pores could overcome the limitations of traditional nanofiltration (NF) membranes, which are typically composed for amorphous polymers and suffer from disordered pore structures and reduced solvent permeability. Incorporating these crystalline materials into NF membranes, we offer a promising solution to enhance both permeability and selectivity, potentially revolutionizing molecular separation processes.

References

[1] de Silva P., Corminboeuf C. Simultaneous Visualization of Covalent and Noncovalent Interactions Using Regions of Density Overlap. *J. Chem. Theory Comput.*, 2014, **10**, P. 3745–3756.

[2] Johnson E.R., Keinan S., Mori-Sánchez P., Contreras-García J., Cohen A.J., Yang W. Revealing Noncovalent Interactions. *J. Am. Chem. Soc.*, 2010, **132**, P. 6498–6506.

[3] Andrezálová L., Országhová Z. Covalent and noncovalent interactions of coordination compounds with DNA: An overview. *Journal of Inorganic Biochemistry*, 2021, **225**, P. 111624.

[4] Gao X., Zou X., Ma H., Meng S., Zhu G. Highly Selective and Permeable Porous Organic Framework Membrane for CO_2 Capture. *Advanced Materials*, 2014, **26**, P. 3644–3648.

[5] Hobza P., ŘezáčJ. Introduction: Noncovalent Interactions. *Chem. Rev.*, 2016, **116**, P. 4911–4912.

[6] Kollman P.A. Noncovalent interactions. *Acc. Chem. Res.*, 1977, **10**, P. 365–371.

[7] Vyas V.S., Vishwakarma M., Moudrakovski I., Haase F., Savasci G., Ochsenfeld C., Spatz J.P., Lotsch B.V. Exploiting Noncovalent Interactions in an Imine-Based Covalent Organic Framework for Quercetin Delivery. *Advanced Materials*, 2016, **28**, P. 8749–8754.

[8] Li P., Ryder M.R., Stoddart J.F. Hydrogen-Bonded Organic Frameworks: A Rising Class of Porous Molecular Materials. *Acc. Mater. Res.*, 2020, **1**, P. 77–87.

[9] Shah M., McCarthy M.C., Sachdeva S., Lee A.K., Jeong H.-K. Current Status of Metal–Organic Framework Membranes for Gas Separations: Promises and Challenges. *Ind. Eng. Chem. Res.*, 2012, **51**, P. 2179–2199.

[10] Caro J., Noack M. Zeolite membranes – Recent developments and progress. *Microporous and Mesoporous Materials*, 2008, **115**, P. 215–233.

[11] Zhu X., Tian C., Mahurin S.M., Chai S.-H., Wang C., Brown S., Veith G.M., Luo H., Liu H., Dai S. A Superacid-Catalyzed Synthesis of Porous Membranes Based on Triazine Frameworks for CO2 Separation. *J. Am. Chem. Soc.*, 2012, **134**, P. 10478–10484.

[12] Carta M., Malpass-Evans R., Croad M., Rogan Y., Jansen J.C., Bernardo P., Bazzarelli F., McKeown N.B. An Efficient Polymer Molecular Sieve for Membrane Gas Separations. *Science*, 2013, **339**, P. 303–307.

[13] Chen L., Zhang B., Chen L., Liu H., Hu Y., Qiao S. Hydrogen-bonded organic frameworks: design, applications, and prospects. *Mater. Adv.*, 2022, **3**, P. 3680–3708.

[14] Yang J., Wang J., Hou B., Huang X., Wang T., Bao Y., Hao H. Porous hydrogen-bonded organic frameworks (HOFs): From design to potential applications. *Chemical Engineering Journal*, 2020, **399**, P. 125873.

[15] Arduengo A.J.I., Gamper S.F., Tamm M., Calabrese J.C., Davidson F., Craig H.A. A Bis(carbene)-Proton Complex: Structure of a C-H-C Hydrogen Bond. *J. Am. Chem. Soc.*, 1995, **117**, P. 572–573.

[16] Gronert S., Keeffe J.R. Identity Hydride-Ion Transfer from C?H Donors to C Acceptor Sites. Enthalpies of Hydride Addition and Enthalpies of Activation. Comparison with C$\cdots$H$\cdots$C Proton Transfer. An ab Initio Study. *J. Am. Chem. Soc.*, 2005, **127**, P. 2324–2333.

[17] Krishnamohan Sharma C.V., Broker G.A., Rogers R.D. Polymorphous One-Dimensional Tetrapyridylporphyrin Coordination Polymers Which Structurally Mimic Aryl Stacking Interactions. *Journal of Solid State Chemistry*, 2000, **152**, P. 253–260.

[18] Duarte M.T., Piedade M.F.M., Robalo M.P., Teixeira A.P.S., Garcia M.H. A supramolecular zigzag chain of organometallic dipoles mediated by PF6-anions. *Acta Crystallogr C Cryst Struct Commun*, 2005, **61**, P. m386–m389.

[19] Das S., Bharadwaj P.K. Self-Assembly of a Luminescent Zinc(II) Complex: a Supramolecular Host–Guest Fluorescence Signaling System for Selective Nitrobenzene Inclusion. *Inorg. Chem.*, 2006, **45**, P. 5257–5259.

[20] Chakravorty S., Platts J.A., Das B.K. Novel C–H$\cdots$C contacts involving 3,5-dimethylpyrazole ligands in a tetracoordinate Co(ii) complex. *Dalton Trans.*, 2011, **40**, P. 11605.

[21] Kharel S., Bhuvanesh N., Gladysz J.A., Blümel J. New hydrogen bonding motifs of phosphine oxides with a silanediol, a phenol, and chloroform. *Inorganica Chimica Acta*, 2019, **490**, P. 215–219.

[22] Tupikina E.Yu., Bodensteiner M., Tolstoy P.M., Denisov G.S., Shenderovich I.G. P=O Moiety as an Ambidextrous Hydrogen Bond Acceptor. *J. Phys. Chem. C*, 2018, **122**, P. 711–1720.

[23] Kostin M.A., Pylaeva S.A., Tolstoy P.M. Phosphine oxides as NMR and IR spectroscopic probes for the estimation of the geometry and energy of PO$\cdots$H–A hydrogen bonds. *Phys. Chem. Chem. Phys.*, 2022, **24**, P. 7121–7133.

[24] Kostin M.A., Alkhuder O., Xu L., Krutin D.V., Asfin R.E., Tolstoy P.M. Complexes of phosphine oxides with substituted phenols: hydrogen bond characterization based on shifts of P-O stretching bands. *Phys. Chem. Chem. Phys.*, 2024, **26**, P. 10234–10242.

[25] Gafurov Z.N., Zueva E.M., Yakhvarov D.G. Sustainable Synthesis, NMR and Computational Study of Isobutylmesitylphosphine. *Chemistry Select*, 2021, **6**, P. 1833–1837.

[26] Jerphagnon T., Renaud J.-L., Bruneau C. Chiral monodentate phosphorus ligands for rhodium-catalyzed asymmetric hydrogenation. *Tetrahedron: Asymmetry*, 2004, **15**, P. 2101–2111.

[27] Imamoto T., Crépy K.V.L., Katagiri K. Optically active 1,1'-di-tert-butyl-2,2'-dibenzophosphetenyl: a highly strained P-stereogenic diphosphine ligand. *Tetrahedron: Asymmetry*, 2004, **15**, P. 2213–2218.

[28] Cheng X., Horton P.N., Hursthouse M.B., Hii K.K. Aminohydroxy phosphine oxide ligands in ruthenium-catalysed asymmetric transfer hydrogenation reactions. *Tetrahedron: Asymmetry*, 2004, **15**, P. 2241–2246.

[29] Methot J.L., Roush W.R. Nucleophilic Phosphine Organocatalysis. *Adv Synth Catal*, 2004, 346, P. 1035–1050.

[30] Seayad J., List B. Asymmetric organocatalysis. *Org. Biomol. Chem.*, 2005, **3**, P. 719.

[31] Connon S.J. Chiral Phosphoric Acids: Powerful Organocatalysts for Asymmetric Addition Reactions to Imines. *Angew Chem Int Ed*, 2006, **45**, P. 3909–3912.

[32] Benaglia M., Rossi S. Chiral phosphine oxides in present-day organocatalysis. *Org. Biomol. Chem.*, 2010, **8**, P. 3824.

[33] Adams H., Collins R.C., Jones S., Warner C.J.A. Enantioselective Preparation of P-Chiral Phosphine Oxides. *Org. Lett.*, 2011, **13**, P. 6576–6579.

[34] Gafurov Z.N., Musin L.I., Sakhapov I.F., Babaev V.M., Musina E.I., Karasik A.A., Sinyashin O.G., Yakhvarov D.G. The formation of secondary arylphosphines in the reaction of organonickel sigma-complex [NiBr(Mes)(bpy)], where Mes = 2,4,6-trimethylphenyl, bpy = 2,2'-bipyridine, with phenylphosphine. *Phosphorus, Sulfur, and Silicon and the Related Elements*, 2016, **191**, P. 1475–1477.

[35] Sheldrick G.M. SHELXT– Integrated space-group and crystal-structure determination. *Acta Crystallogr A Found Adv*, 2015, **71**, P. 3–8.

[36] Sheldrick G.M. A short history of SHELX. *Acta Crystallogr A Found Crystallogr*, 2007, **64**, P. 112–122.

[37] Macrae C.F. Edgington P.R., McCabe P., Pidcock E., Shields G.P., Taylor R., Towler M., Van De Streek J. Mercury: visualization and analysis of crystal structures. *J Appl Crystallogr*, 2006, **39**, P. 453–457.

[38] www.ccdc.cam.ac.uk/conts/retrieving.html (or from the Cambridge Crystallographic Data Centre, 12 Union Road, Cambridge CB2 1EZ, UK; fax: (+44) 1223-336-033; or deposit@ccdc.cam.uk)

[39] EVA v.11.0.0.3. User Manual. SOCABIM, 2005.

[40] Spackman P.R., Turner M.J., McKinnon J.J., Wolff S.K., Grimwood D.J., Jayatilaka D., Spackman M.A. CrystalExplorer: a program for Hirshfeld surface analysis, visualization and quantitative analysis of molecular crystals. *J Appl Crystallogr*, 2021, **54**, P. 1006–1011.

[41] Mackenzie C.F., Spackman P.R., Jayatilaka D., Spackman M.A. CrystalExplorer model energies and energy frameworks: extension to metal coordination compounds, organic salts, solvates and open-shell systems. *IUCrJ*, 2017, **4**, P. 575–587.

[42] Grossmann G., Krüger K., Ohms G., Fischer A., Jones P.G., Goerlich J., Schmutzler R. Phosphorus Nuclear Magnetic Shielding Anisotropy and Crystal Structure of (1-Hydroxyalkyl)dimethylphosphine Sulfides. *Inorg. Chem.*, 1997, **36**, P. 770–775.

Information about the authors:

Alexey A. Kagilev – Arbuzov Institute of Organic and Physical Chemistry, FRC Kazan Scientific Center, Russian Academy of Sciences, 420088, Kazan, Russian Federation; ORCID 0000-0002-5603-1311; al-kagilev@mail.ru

Ilyas F. Sakhapov – Arbuzov Institute of Organic and Physical Chemistry, FRC Kazan Scientific Center, Russian Academy of Sciences, 420088, Kazan, Russian Federation; ORCID 0000-0002-7440-1486; ilyas.sakhapov@iopc.ru

Zufar N. Gafurov – Arbuzov Institute of Organic and Physical Chemistry, FRC Kazan Scientific Center, Russian Academy of Sciences, 420088, Kazan, Russian Federation; ORCID 0000-0001-6615-8968; gafurov.zufar@iopc.ru

Artyom O. Kantyukov – Arbuzov Institute of Organic and Physical Chemistry, FRC Kazan Scientific Center, Russian Academy of Sciences, 420088, Kazan, Russian Federation; A.M. Butlerov Institute of Chemistry, Kazan Federal University, 420008, Kazan, Russian Federation; ORCID 0000-0002-2285-300X; kant.art@mail.ru

Ilya K. Mikhailov – Arbuzov Institute of Organic and Physical Chemistry, FRC Kazan Scientific Center, Russian Academy of Sciences, 420088, Kazan, Russian Federation; ORCID 0000-0001-9373-2996; tiimhailovilya@gmail.com

Daut R. Islamov – Laboratory for Structural Studies of Biomacromolecules, FRC Kazan Scientific Center, Russian Academy of Sciences, 420111, Kazan, Russian Federation; ORCID 0000-0002-5988-1012; daut1989@mail.ru

Alexander V. Gerasimov – A.M. Butlerov Institute of Chemistry, Kazan Federal University, 420008, Kazan, Russian Federation; ORCID 0000-0003-4213-9724; Alexander.Gerasimov@kpfu.ru

Oleg A. Filippov – A.N. Nesmeyanov Institute of Organoelement Compounds, Russian Academy of Sciences, 119991, Moscow, Russian Federation; ORCID 0000-0002-7963-2806; h-bond@ineos.ac.ru

Aidar T. Gubaidullin – Arbuzov Institute of Organic and Physical Chemistry, FRC Kazan Scientific Center, Russian Academy of Sciences, 420088, Kazan, Russian Federation; ORCID 0000-0002-8114-7025; aidar@iopc.ru

Olga S. Soficheva – Arbuzov Institute of Organic and Physical Chemistry, FRC Kazan Scientific Center, Russian Academy of Sciences, 420088, Kazan, Russian Federation; ORCID 0000-0003-3107-5251; myaolechka@yandex.ru

Oleg G. Sinyashin – Arbuzov Institute of Organic and Physical Chemistry, FRC Kazan Scientific Center, Russian Academy of Sciences, 420088, Kazan, Russian Federation; ORCID 0000-0002-2241-9764; oleg@iopc.ru

Dmitry G. Yakhvarov – Arbuzov Institute of Organic and Physical Chemistry, FRC Kazan Scientific Center, Russian Academy of Sciences, 420088, Kazan, Russian Federation; A.M. Butlerov Institute of Chemistry, Kazan Federal University, 420008, Kazan, Russian Federation; ORCID 0000-0002-3906-8841; yakhvar@iopc.ru